Fracture resistance of wood adhesive bonds: Experimental insights into the J-integral approach using acoustic emission testing

IOP Conf. Series: Materials Science and Engineering **1338** (2025) 012005 doi:10.1088/1757-899X/1338/1/012005

Fracture resistance of wood adhesive bonds: Experimental insights into the J-integral approach using acoustic emission testing

Joran van Blokland[1*], Ruben I. Erives[2], Ashish K. Bangaru[2], Malcolm McGugan[2] and Bent F. Sørensen[2]

[1] Division of Wood Science and Technology, Swedish University of Agricultural Sciences, Uppsala, Sweden
[2] Department of Wind and Energy Systems, Technical University of Denmark, Roskilde, Denmark

[*]E-mail: joran.van.blokland@slu.se

Abstract. Acoustic emission (AE) measurements were used to detect the onset of crack initiation and propagation, as well as to monitor crack front advancement during fracture resistance tests on wood-adhesive bonds. In parallel, digital image correlation (DIC) was employed as an independent technique to also monitor crack front progression. These measurements were conducted with the aim of further adapting and developing the J-integral approach for fracture characterisation of wood and wood-adhesive joints. In this method, double cantilever beam (DCB) specimens are loaded under pure bending moments to determine R-curves and cohesive laws. Tests were performed on European beech wood specimens bonded with a bio-based wood–lignin adhesive. The results show that AE can effectively identify the onset of crack initiation and propagation, supporting the characterisation and interpretation of R-curve and cohesive law data. Additionally, both AE-based localisation and DIC-derived strain fields can be used to estimate the cohesive zone length during crack growth.

1. Introduction

Wood-based materials can contribute to the sustainable development of the wind energy sector by providing environmental benefits and offer improved recyclability [1]. In 2023, a 105-meter-tall wooden tower was constructed from laminated veneer lumber (LVL) made of spruce (the same species commonly used as Christmas trees). Thanks to its lightweight, high strength, and renewable origin, LVL significantly contributed to the carbon neutrality of the wind energy system [2]. Wood, particularly balsa and LVL, is also being integrated into wind turbine blades as a cost-effective, low-carbon alternative to traditional fibreglass and carbon composites [3]. Moreover, wooden components offer logistical advantages, such as easier overland transportation compared to conventional materials [2]. Despite these advantages, engineering with wood presents specific challenges. One of the key issues is predicting its mechanical behaviour under various loading conditions, in particular its response to fracture.

Traditionally, linear elastic fracture mechanics (LEFM) has been used to evaluate fracture properties of wood and wood-adhesive bonds [4]. However, wood often exhibits non-linear softening behaviour due to damage mechanisms like fibre bridging, making cohesive zone models a more suitable framework for characterisation [5]. The J-integral approach—where a double cantilever beam (DCB) specimen is loaded with pure bending moments—has been successfully used to characterise cohesive laws in fibre-reinforced composites and adhesive joints within the wind energy sector [6]. However, it has only recently been applied to wood and wood-adhesive systems [7].

Crack initiation, also known as crack onset, refers to the point at which a delamination crack first forms, while steady-state crack propagation describes the stage where the fracture process zone is fully developed and the crack advances at an approximately constant rate. From the perspective of deriving cohesive laws, identifying these two stages is valuable because it enables fitting of different functional forms (and thus different derivatives, i.e., tractions) to the R-curves, as demonstrated in [8]. Moreover, these measurements correspond to physical processes that may be relevant to specific design criteria—for example, *J* at crack onset can be related to a no-growth criterion, while the steady-state *J* value can be taken as a material parameter that informs criteria for stable (slow) crack growth.

This study aims to further adapt the J-integral approach for extracting R-curves of wood-adhesive bonds. For this purpose, an experimental campaign was conducted on DCB specimens of wood-adhesive joints under nominal mode I loading. Acoustic emission (AE) was used to detect the onset of crack initiation and steady-state crack propagation, and to track crack front progression. Digital image correlation (DIC) was employed as a complementary technique to validate and support the AE-based identification of crack front progression. The focus of the study is on method development, building on techniques previously applied to investigate delamination in fibreglass and carbon fibre composites [8, 9]. The scope was limited to a single specimen of European beech wood bonded with a bio-based wood-lignin adhesive.

2. Materials

2.1 Veneer preparation

A veneer sheet of European beech (*Fagus sylvatica*) with a thickness of 2.4 mm was used. The air-dry density of the wood was 726 kg/m^3, measured after conditioning the specimen at 65% relative humidity and 20 °C—conditions that correspond to service class 1, as defined by European design standards for timber—until weight stabilisation [10, 11]. The sheet was stored indoors before gluing and had a wood moisture content of approximately 5–6% prior to bonding.

The surface to be glued is the radial–longitudinal plane, which enables crack growth in the tangential–longitudinal (TL) direction along the intended bond line. The veneer was oriented with the out-of-plane fibre direction angled toward the bond line, as described earlier by [7]. A 12 µm thick release film (VAClease R1.2, VAC Innovation Ltd) was adhered to one side of the veneer using a thin layer of spray adhesive to define the crack initiation plane.

2.2 Gluing and pressing

A wood-lignin bio-based adhesive, developed by Stora Enso AB, was used. The adhesive was applied at a spread rate of 130 g/m^2 to one side of the veneer. The lay-up was pressed in a hot press (LAP 200, Gottfried Joos Maschinenfabrik GmbH & Co. KG, Pfalzgrafenweiler, Germany) at 120 °C for 130 seconds, using a press factor slightly above 30 mm/s. The wood moisture content increased during this step. After pressing, the glue-up was post-cured for 24 hours and then stored under service class 1 conditions.

2.3 DCB specimens

Smoothly surfaced (planed), small-dimension, high-quality pine timber (*Pinus sylvestris*) was used to construct the double cantilever beam (DCB) specimen, targeting a beam stiffness (EI) of approximately 800 Nm^2. To achieve this, two pine pieces, each 15 mm thick, were glued to either side of the veneer lay-up using a polyvinyl acetate-based (PVAc) wood adhesive (Cascol Indoor, Casco). After gluing and post-curing, the specimen was stored under service class 1 conditions before being cut to their final dimensions: 500 mm in length and 30 mm in width (*b*). The total height (i.e. twice the beam height, *H*) was between 64 and 65 mm.

The final lay-up sequence of the DCB specimen was: pine$_{15}$ / PVAc adhesive$_{0.01}$ / pine$_{15}$ / PVAc adhesive$_{0.01}$ / beech-veneer$_{2.4}$ / lignin adhesive$_{0.01}$ / release film$_{0.012}$ / beech veneer$_{2.4}$ / PVAc adhesive$_{0.01}$ / pine$_{15}$ / PVAc adhesive$_{0.01}$ / pine$_{15}$. Subscripts indicate approximate layer thicknesses in mm; bond-line thicknesses were not measured.

To enable load application, two aluminium tabs were attached to the specimen using a gel-type cyanoacrylate adhesive (Expres Gel, Casco), suitable for bonding wood to metal, and secured with screws. Finally, a speckle pattern for digital image correlation (DIC) analysis was applied by first spraying a white base coat, followed by a fine black spatter. The specimen was stored at service class 1 conditions until testing.

3. Methods

3.1 DCB testing

The DCB specimen was loaded by applying bending moments to the beam ends using a custom-made setup developed at the Department of Wind and Energy Systems at the Technical University of Denmark [6]. The setup employs a system of levers and pulleys actuated by the movement of a crosshead beam. Equal and opposite moments were applied to each beam end to produce nominal mode I loading, with the specimen supported at the bottom (Figure 1). A detailed description of the setup relevant to this work is available in [7]. The loading speed of the crosshead beam was set to 2 mm/min, targeting peak traction after 1–2 minutes. Applied moment (M) and time (t) signals were recorded at 10 Hz. The overall test progression was recorded on video from the back side (Figure 1a), while a front-facing camera captured images for DIC (Figure 1b), as further described in Section 2.3. The test was stopped once the crack tip reached a distance equal to three times the beam height above the bottom support. Moisture content at the time of testing was measured using the oven-dry method [11].

3.2 Acoustic emission

For acoustic emission (AE) measurements, two R15α narrow-band resonant piezoelectric sensors (Physical Acoustics Corporation) were attached to one of the beams. The first sensor was positioned 10 mm above the crack initiation plane, and the second was placed 100 mm further along the beam length (Figure 1a). In addition to enabling linear localisation of AE events along this distance, the system recorded cumulative energy and cumulative hit counts to monitor the progression of damage.

3.3 Digital image correlation

An area of 67 mm across the specimen by 100 mm along the specimen (4000 × 6000 pixels) around the crack initiation region was recorded using a camera (Nikon D7200, Nikon AF-S NIKKOR 18–200 mm f/3.5–5.6 lens) at 0.5 Hz during testing (Figure 1b). Camera settings were: aperture F/8, shutter speed 1/40 s, ISO 250, and focal length 200 mm. The images were reduced to one frame every 4 seconds and imported into ARAMIS (GOM GmbH) to extract end-opening displacements (δ), beam curvature (κ), and to plot strain fields (ε_y). The virtual extensometer was positioned at the crack initiation plane, 75 mm from the top of the metal block, spanning from the neutral axis of beam 1 to that of beam 2—corresponding to an approximate gauge length of 32 mm (Figure 1b). The analysis was performed using 2D DIC, applying quadrangle facets with a facet (face) size of 50 pixels and a point distance of 25 pixels. Strains were calculated using a linear strain

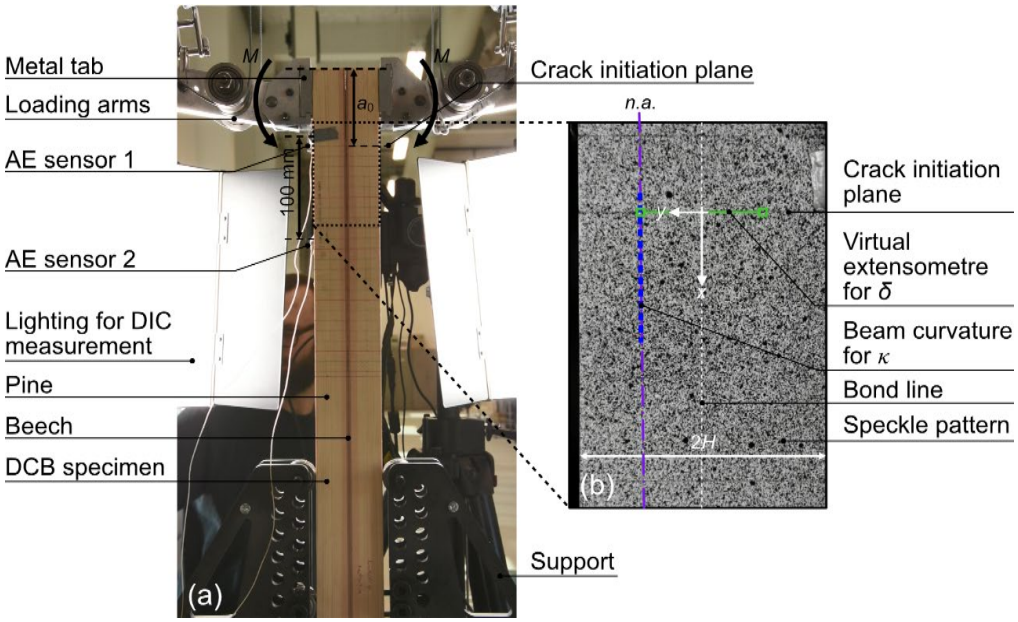

Figure 1. DCB testing: (a) overview of setup (back-side of setup), and (b) DIC measurement (front-side).

computation method, with an estimated reference length of 0.4 mm. Facet matching was performed against the previous stage.

3.4 Data analysis

3.4.1 R-curves and cohesive laws

The external J-integral was calculated using a closed-form solution as [6]: $J = (1-\upsilon^2)\frac{M^2}{b \cdot EI}$, where ν was taken as 0.5, and EI was derived from the measured moment M and beam curvature κ. Plane strain at the crack tip was assumed because the DCB has thick, wide adherents (b = 30 mm, H = 32 mm per arm) and a very thin bond line (presumably, <0.1 mm), which provide strong through-thickness constraint and suppress lateral contraction. Cohesive laws—i.e., the relationship between the traction in the cohesive zone, σ, and the end-opening displacement, δ—were obtained by numerical differentiation of the R-curves (J–δ) using a piecewise linear fitting approach. For a more detailed description of the data reduction procedure, see [7].

3.4.2 Crack initiation and propagation onset

AE measurements were used to identify the onset time of crack initiation, t_0, and the onset time of steady-state crack propagation, t_{ss}. Identification of t_0 and t_{ss} were based on visual assessment of plots of cumulative AE measurements (energy and hit counts) versus time and end-opening displacement, following a similar approach to that previously applied to glass-epoxy composites [8]. In that earlier work, distinct regions were identified, separated by noticeable kinks in the curve that marked the transitions between them.

3.4.3 Cohesive zone length during crack growth

In previous work on glass–epoxy composites, localisation data plotted against time was used to determine the position of the crack tip and roughly estimate the fracture process zone as a function of testing time [9]. Surface strain (ε_y) perpendicular to the direction of crack propagation measured with DIC has also been used for crack localisation in wood [12]. The approaches described in [9] and [12] have been applied here. Localisation from AE measurements and strain fields from DIC measurements were used to track the propagation of the crack front. By measuring from the crack initiation plane, the length of the cohesive zone, ℓ, was determined up to the time t_{ss}, when steady-state crack propagation begins. Here, ℓ_0 refers to the cohesive zone length at crack initiation time t_0, while ℓ_{ss} denotes the fully developed cohesive zone length at t_{ss}.

4. Results & Discussion

The results presented here derive from the double-cantilever-beam (DCB) test on the beech-veneer–lignin adhesive bond line described in the Materials section. This study forms part of a broader programme that will include larger sample sizes, additional adhesives, and other wood species. Here we report an initial

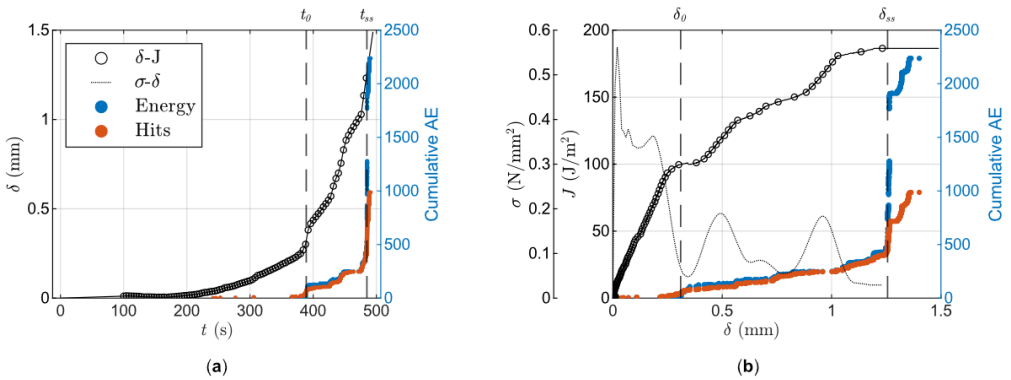

Figure 2. Results DCB and AE testing: (a) end-opening δ and cumulative AE versus time, and (b) fracture resistance J and cohesive stress σ and cumulative AE versus end-opening δ.

proof-of-concept based on a single, well-controlled and representative specimen to demonstrate the applicability of the methods to wood and wood–adhesive interfaces.

4.1 R-curves and cohesive laws

Figure 2a (left) shows the progression of end opening over time, along with the cumulative acoustic emission (AE) energy and hit count. Figure 2b (right) displays the corresponding R-curve and traction plotted against end opening, together with the cumulative AE energy and hit count. Starting with the R-curve: it is fairly smooth, indicating stable fracture development, with steady-state reached at around 180 J/m^2 at an end-opening displacement of approximately 1 mm. The shape of the cohesive law shows a distinct peak traction of 0.56 N/mm^2 at a very small deformation of 0.02 mm, and the area under the curve—corresponding to the fracture energy release rate—was found to be 184 J/m^2. The total test duration was approximately 8 minutes. The initial loading phase, up to a J-value of 2 J/m^2 (about 1% of the maximum), took 2 min and 16 s. Subtracting this from the time to peak load shows that it took 1 min and 16 s to reach peak stress. The average loading rate—defined as end-opening displacement over time—was 0.011 mm/min.

4.2 Crack initiation and propagation onset

From the cumulative AE data for hits and energy shown in Figure 2, three distinct regions can be identified, separated by two noticeable kinks. In the first region, only minimal AE activity is observed. In the second region, cumulative AE energy and hit counts increase steadily. In the final region, a pronounced rise in AE activity occurs. By plotting cumulative AE data alongside end-opening displacement (Figure 2a) and alongside J and σ (Figure 2b), it becomes clear that the first kink corresponds to a rapid increase in end opening, which indicates that a crack front has formed and the beams begin to separate. The second kink aligns with the point where the J–δ curve begins to level off. These observations support the identification of the onset time of crack initiation, t_0, and the onset of crack propagation, t_{ss}, with these two kinks. Both points are indicated in Figure 2 by dashed vertical lines. Table 1 summarises these results, including the corresponding values of J and δ at t_0 (389 s) and t_{ss} (485 s).

4.3 Cohesive zone length during crack growth

Figure 3 shows the AE-based localisation data based on the triangulation of the energy/hits. The y-axis represents the position of AE events relative to the crack initiation plane 'Location' (in mm), while the x-axis shows testing time t (in s). The previously identified times for crack initiation (t_0) and the onset of crack propagation (t_{ss}) are marked with dashed vertical lines. Although the localisation points are scattered—ranging from approximately −10 mm (sensor 1) to 90 mm (sensor 2)—a general trend of crack front advancement can be observed. Two vertical bands of higher point density are clearly visible and correspond well with the events at t_0 and t_{ss}. To further quantify the trend, a linear regression was applied to the localisation data (solid black line in Figure 3). The intersections of this trend line with the dashed lines provide estimates of the cohesive zone length based on AE measurements: $\ell_{0,AE} \approx 40$ mm at t_0, and $\ell_{ss,AE} \approx 60$ mm at t_{ss}, as summarised in Table 1.

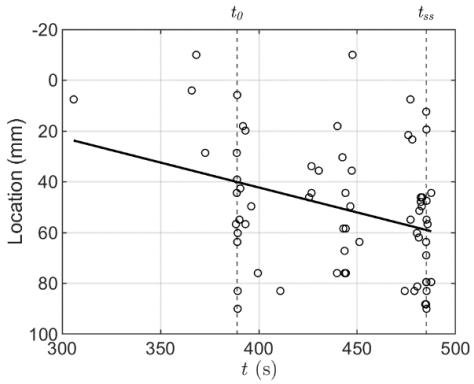

Figure 3. Localisation from AE testing

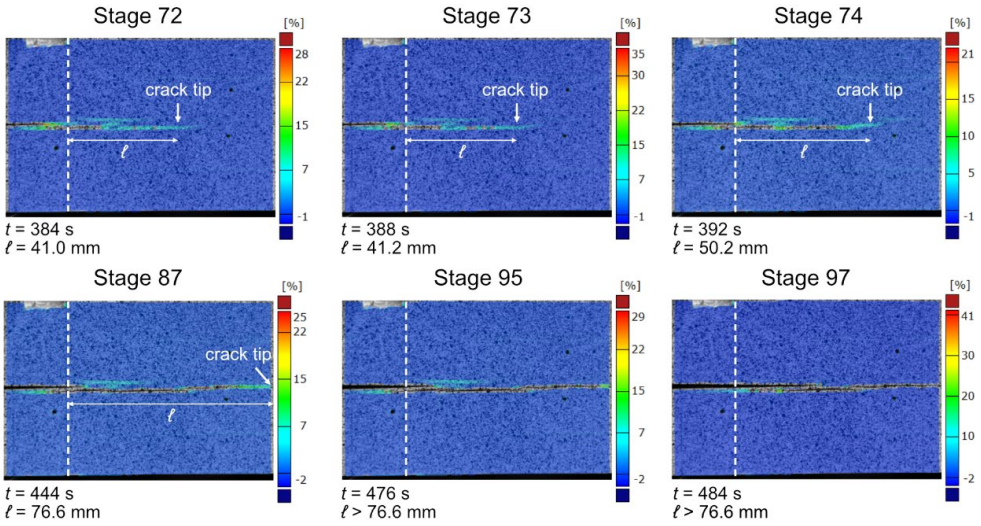

Figure 4. Surface strain (ε_y) at various load stages

Figure 4 shows the surface strain fields obtained from DIC measurements at various load stages. The colour scale indicates strain magnitude in percent. The crack tip is marked by a white arrow, and the estimated length of the cohesive zone at each stage, ℓ_{DIC}, is shown by a double-headed arrow. For each stage, the corresponding testing time t (in s) and cohesive zone length ℓ (in mm) are also provided. Stages 72–74 correspond to the period around crack initiation (t_0). Here, $\ell_{0,DIC}$ is approximately 41 mm (Table 1). At stage 87 (444 s), the crack front reaches the edge of the field of view and is approximately 77 mm. Stages 95 and 97 are associated with the onset steady-state crack propagation (t_{ss}). Since the crack has propagated beyond the field of view, $\ell_{ss,DIC}$ could not be identified but is at least 77 mm (Table 1).

Both methods—AE and DIC—used to determine the cohesive zone length during crack growth showed good agreement for ℓ at t_0, increasing confidence in the results (Table 1). However, at t_{ss}, there was a notable discrepancy between the two methods. While DIC could not provide an accurate measurement at this stage—because the crack propagated beyond the field of view—the difference between the AE and DIC estimates is at least 16 mm, corresponding to a deviation of at least 27%. Uncertainty in AE-based localisation measurements arises from the fact that micro-cracking may occur away from the main crack tip (e.g. in areas of elevated strain in Figure 4, parallel to the main crack path), contributing to scatter in the localisation data. There are multiple methods to segregate/categorise AE data to their corresponding damage mechanism, however these methods require extensive data from different experiments as well as extensive knowledge of the material [13]. On the other hand, AE captures all activity within the measured volume, while DIC is limited to surface observations. It is known that the crack front can vary across the specimen width, so the front on the opposite side may have developed differently, contributing to the observed differences. Further efforts to increase the sample size and to analyse ℓ_{DIC} as a function of time are warranted.

5. Conclusions

This study aimed to further adapt and develop the J-integral approach for extracting R-curves and cohesive laws of wood-adhesive bonds by simultaneously using acoustic emission (AE) and digital image correlation (DIC) measurements during testing. Based on the presented results, the following conclusions can be drawn:

- AE measurements are a valuable tool for identifying crack initiation and the onset of crack propagation during double cantilever beam (DCB) mode I tests on adhesive-bonded wood, supporting the characterisation of R-curves and cohesive law data.
- Both AE-based localisation and DIC can be used to determine the cohesive zone length ℓ during crack growth in fracture mechanical tests on adhesive-bonded wood.

Further efforts to increase the sample size and to analyse ℓ from DIC as a function of time are warranted. The results from this work contribute to refining experimental protocols for R-curve measurement and

cohesive law derivation in wood and wood–adhesive bonds. These insights support the expanded use of engineered wood products (EWPs), such as laminated veneer lumber (LVL), in advanced engineering applications (e.g., turbine blade cores and wooden towers), thereby promoting sustainable development in the wind energy sector through the integration of renewable materials.

Table 1. Results

Crack initiation		
t_0	s	389
δ_0	mm	0.310
J_0	J/m^2	100
Steady state		
t_{ss}	s	485
δ_{ss}	mm	1.232[a]
J_{ss}	J/m^2	186[a]
Fracture process zone		
$\ell_{0,AE}$	mm	40
$\ell_{0,DIC}$	mm	41
$\ell_{ss,AE}$	mm	60
$\ell_{ss,DIC}$	mm	>76

[a] taken a t = 484 s.

6. Acknowledgement

This study received financial support from Svenska Forskningsrådet Formas, the Swedish Research Council for Sustainable Development, under the project titled “Framework for development and implementation of biobased wood adhesive systems through fracture mechanical testing” (grant no. 2022-00529). Additional support was provided by the project “Crack Kinking in Composites (CraKinC),” funded by the Independent Research Fund Denmark, Technology and Production Sciences (case no. 4286-00302B). The lignin-based adhesive and hardener used in this research were generously supplied by Stora Enso AB.

References

[1] Holttinen H, Mälkki H, Turkulainen T, Bijsterbosch H and Schmidt R 1999 Life cycle assessment of different wind turbine blade materials *1999 European Wind Energy Conference* ed EL Petersen (Routledge)]
[2] Sara 2023 World’s tallest wooden wind turbine tower being built in Sweden (Press release) *Modvion* [Retrieved from https://modvion.com/news/worlds-tallest-wooden-wind-turbine-tower-being-built-in-sweden/#:~:text=A%20105%2Dmeter%20wind%20turbine,make%20up%20the%20finished%20tower]
[3] Cathrine Wallenius 2022 Stora Enso forms partnership with Voodin Blades to develop sustainable wind turbine blades from wood (Press release) *StoraEnso* [Retrieved from https://www.storaenso.com/en/newsroom/press-releases/2022/11/stora-enso-forms-partnership-with-voodin-blades-to-develop-sustainable-wind-turbine-blades-from-wood]
[4] River BH 1994 Fracture of adhesive-bonded wood joints *Handbook of Adhesive Technology* eds A Pizzi and KL Mittal (New york: Marcal Dekker Inc)
[5] Gómez-Royuela JL, Majano-Majano A, Lara-Bocanegra AJ, Xavier J and de Moura MFSF 2022 *THEOR APPL FRACT MEC* **118** 103220
[6] Sørensen BF 2010 Cohesive laws for assessment of materials failure: Theory, experimental methods and application *Doctor Technices* Technical University of Denmark, Denmark
[7] Van Blokland J, Sørensen BF, Serrano E, Gamstedt EK and Erives RI 2025 Measuring cohesive law of wood adhesive bonds for engineering of timber joints and products *World Conference on Timber Engineering 2025* (Brisbane) p 1687-1696 [https://doi.org/10.52202/080513-0206]
[8] Erives R, Sørensen BF and Goutianos S 2023 *Compos Part A: Appl Sci Manuf* **165** 107346
[9] Erives RI, Bangaru AK and McGugan M 2024 Procedia Struct Integr **52** 600-610
[10] Eurocode 5 *2014 Design of timber structures – Part 1-1: General – Common Rules and Rules for Buildings* (Brussels: CEN European Committee for Standardization)
[11] ISO 13061-1 2014 *Physical and Mechanical Properties of Wood — Test Methods for Small Clear Wood Specimens — Part 1: Determination of Moisture Content for Physical and Mechanical Tests* (Switzerland: ISO)
[12] van Blokland J, Olsson A, Oscarsson J, Daniel G and Adamopoulos S 2020 *Wood Sci Technol* **54**(4) 1001-1028
[13] Muir C, Swaminathan B, Almansour AS, Sevener K, Smith C, Presby M, Kiser JD, Pollock TM and Daly S 2021 *npj Comput Mater* **7** 95